COBEM 2023 27TH INTERNATIONAL CONGRESS OF MECHANICAL ENGENEERING

ABCM Brazilian Society of Mechanical Sciences and Engineering
27th ABCM International Congress of Mechanical Engineering
December 04-08, 2023, Florianópolis-SC, Brazil

COB-2023-0361
INVESTIGATIONS ON ENHANCING HARDENING OF CuNi ELECTRODEPOSITED COATINGS OBTAINED IN THE PRESENCE OF MICRO-Al_2O_3 PARTICLES IN A CITRATE-AMMONIA SOLUTION.

Paulo Cezar Tulio
Federal University of Technology (UTFPR) – Paraná. 1640 Alberto Carazzai Ave, 86300-000. Cornélio Procópio – Brazil.
e-mail: pauloctulio@utfpr.edu.br

Raphael de Souza
Paula Souza State Center for Technological Education (CEETEPS). 1226 Senhor do Bonfim St, Assis, 19802-130, Brazil.
e-mail: raphael.souza@etec.sp.gov.br

Abstract. *CuNi films were electrodeposited on steel from citrate-ammonia pH 9.2 solutions with and without suspended Al_2O_3 particles (3.4 microns). By microindentation hardness, improved mechanical strength of CuNi coatings obtained from solutions with Al_2O_3 (CuNi(Al)) was observed, especially at high constant cathodic current densities (i_g). No occlusion of Al_2O_3 in the CuNi matrix was verified, but Al_2O_3 particles affected Ni/Cu mass ratio and, therefore, the coating´s properties. At high i_g, CuNi(Al) exhibited higher Ni/Cu mass ratios than CuNi(w) obtained without Al_2O_3 in the solution. X-ray diffraction was performed on the coatings. Through lattice parameter analysis and comparisons with EDS data using empirical Vegard´s law, at high i_g, lattice parameters of CuNi(Al) coatings were smaller than those of CuNi(w), confirming higher Ni content. Since no occlusion of Al_2O_3 was observed in CuNi(Al), improved mechanical properties are explained in terms of the increased Ni content in CuNi(Al) compared to CuNi(w) and solid-solution strengthening. Ni is a metal harder than Cu and Al_2O_3 particles during electrodeposition enhanced hardening by increasing Ni content and not by forming a metal matrix composite at high i_g. Coatings with enhanced mechanical strengthening can be employed for protection against erosion-corrosion.*

Keywords: *CuNi coatings, electrodeposition, Al_2O_3 (alumina), solid-solution strengthening*

1. INTRODUCTION

Nickel is a metal of importance in many technological applications, such as in the production of stainless steels, alloy steel, cast alloys, batteries, and protective coatings (“About nickel | Nickel Institute,” n.d.). As a coating, Ni can be used to protect steel. Many alloys of Ni have good mechanical properties and corrosion resistance (Friend, 1980; Kear et al., 2004). Adding Cu to Ni significantly improves mechanical strength, which is explained by the solid-solution hardening mechanism (Callister, 2007; “Foundry - Lexicon,” n.d.). CuNi forms a miscible solid solution in all compositions due to their very similar chemical and physical properties (Callister, 2007).

For engineering applications, Monel®, a group of CuNi alloys of about 31.5% Cu and 66% Ni with minor elements Fe, Mn, C, and Si (“Monel | alloy | Britannica,” 2007) and 90-10 and 70-30 CuNi are the primary employed (“About nickel | Nickel Institute,” n.d.), especially in seawater media under high-velocity conditions. Alloys of CuNi are found in offshore extraction of oil and gas, desalination plants, power generation, and naval shipping, as propellor shafts, pump impellers, condenser tubes, seawater cooling, firewater systems, and boat hulls (“About nickel | Nickel Institute,” n.d.; Friend, 1980). CuNi alloys with these compositions can be applied as coatings to reduce costs. Many authors developed electrodeposition solutions for CuNi and studied processes involved in its electrodeposition. For the electrodeposition of CuNi, it is necessary a complexing agent. Citrate is a very employed complexing agent (Bigos et al., 2021; Chassaing et al., 1987; Foyet et al., 2007; Lozano-Morales and Podlaha, 2008).

Forming a composite of metal matrix CuNi with a dispersed phase of hard particles such as Al_2O_3 or others can improve surface protective properties. The dispersed phase can improve mechanical strength by dispersion-strengthening, for example. In obtaining composite coatings by electrodeposition, particles must be suspended in the electrodeposition solution before occluding in the matrix. Hydrodynamics control is essential in their obtainment (Hovestad and Janssen, 2005; Tseluikin, 2016). CuNi composite coatings with Al_2O_3 by electrodeposition have been successfully obtained by some authors (Alizadeh and Safaei, 2018; Fawzy et al., 1996; Lozano-Morales and Podlaha, 2008; Panda and Podlaha, 2003). In such investigations, improved mechanical properties were observed, generally expressed in increased microhardness of CuNi-Al_2O_3 composite coatings compared to CuNi. Hardening was mainly attributed to the occluded Al_2O_3 particles, but also grain refinement is observed in some cases. The composition of CuNi matrix can be affected when it is obtained in the presence of Al_2O_3 particles in an electrodeposition solution. Due to this, corrosion resistance

will be affected for CuNi and other binary alloys. However, especially for CuNi, since Ni is harder than Cu, mechanical resistance can also be affected, as it is well-known for cast alloys (Callister, 2007; "Foundry - Lexicon," n.d.). This is not so explored for CuNi composite coatings.

In this work, the hardening of some CuNi coatings obtained by electrodeposition from solutions containing Al_2O_3 particles was investigated in terms of changes in CuNi metal matrix compositions. No occlusion of Al_2O_3 was detected, and a dispersion-strengthening mechanism was not applicable. Solid-solution formation and enhanced content of the harder Ni metal were claimed as possible explanations.

2. EXPERIMENTAL

The CuNi electrodeposition solution was: 0.1 $mol.L^{-1}$ $CuSO_4.5H_2O$, 0.6 $mol.L^{-1}$ $NiSO_4.6H_2O$, 0.7 $mol.L^{-1}$ $Na_3C_6H_5O_7.2H_2O$ (trisodium citrate dihydrate) pH 9.2 adjusted by addition of NH_4OH. This composition was based on (Chassaing et al., 1987). Micrometric α-Al_2O_3 particles, 99.85 % purity, and d_{50} 3.4 μm, were added as-received to this solution up to a mass of Al_2O_3 to the volume of solution ratio (C_P) of 10 $g.L^{-1}$. This electrodeposition solution was previously maintained under magnetic stirring for 12 h to ensure the deagglomeration of particles. Electrodepositions were also performed for C_P of 0 $g.L^{-1}$. Coatings obtained from C_P 10 $g.L^{-1}$ and 0 $g.L^{-1}$ solutions are designated from now on CuNi(Al) and CuNi(w), respectively.

Electrodepositions at room temperature were performed employing a flow-cell, schematically shown in Figure 1.a. The circulation of the solution was maintained through a centrifugal pump, avoiding the sedimentation of Al_2O_3 particles at the bottom of the cell. The impingement of the solution and Al_2O_3 particles was orthogonal against the substrate surface, and the fluid velocity was constant at 0.43 $m.s^{-1}$.

The working electrode substrate (cathode) consisted of rectangular SAE 1020 steel pieces with 5 mm thickness. These were embedded in epoxy resin but with an exposed area to be electrodeposited of 100 mm^2 as shown in Figure 1.b. Before electrodeposition, the surface of the working electrode was sanded up to 600 grit-mesh emery paper, cleaned with acetone, and dried at room temperature. The counter-electrode (anode) was an electrolytic copper rod (ϕ = 9.52 mm) placed laterally to the convergent in the cell.

The constant cathodic current densities (i_g) applied were 25, 40, 60, and 90 $mA.cm^{-2}$. A power source and a multimeter were employed. The charge density was 140.96 $C.cm^{-2}$, corresponding to a theoretical coating thickness of 50 μm.

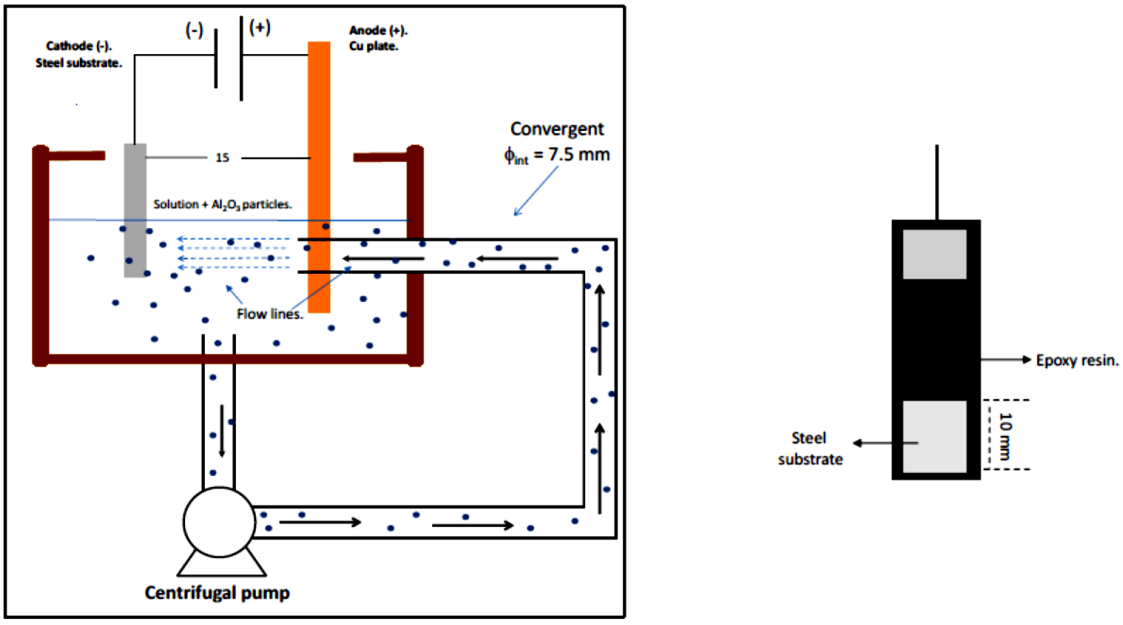

(a) (b)

Figure 1. (a) Schematics of the flow-cell employed; (b) steel electrode (working electrode) configuration.

Scanning Electron Microscopy (SEM) and semiquantitative chemical analysis by EDS employed an FEI Quanta 200 microscope coupled to an EDS-Oxford INCA microanalysis system.

Microindentation hardness tests were performed with a Panambra microhardness tester HV-1000B with the Vickers scale. 50 and 100 gf loads for 15 s were applied. Microindentations were made at distinct areas of the coatings: near the top and bottom edges and at central regions. At least ten indentations in each area were made. The values of Vickers microhardness were converted to MPa.

X-ray diffraction (XRD) data of the coatings were obtained with the D2 Phaser – Bruker diffractometer with 1.54 Å/8.047 keV Cu-Kα1 radiation with angular accuracy of ±0.02° 2θ in all angular range.

3. RESULTS AND DISCUSSION

3.1 Microindentation hardness and EDS analysis

Figure 2 shows microhardness values near the top edge, bottom edge, and central areas of CuNi(w) (C_P 0 g.L^{-1} Al_2O_3) and CuNi(Al) (C_P 10 g.L^{-1} Al_2O_3) coatings as a function of i_g. Also, the dependence of the composition of coatings in each area, expressed by Ni/Cu mass ratio, is evidenced in the plots of Figure 2. The mass ratio Ni/Cu increases with i_g for CuNi(Al) and CuNi(w). Being Ni less noble than Cu, this last dependence was expected since as i_g increases, Ni content in coatings will also increase.

For the data in Figure 2, except for i_g 90 mA.cm^{-2} at the edges, CuNi(Al) coatings exhibited higher microhardness values when compared to CuNi(Al) ones. There is a clear improvement in CuNi(Al) mechanical strengthening at the same i_g compared to CuNi(w). EDS analysis did not detect Al_2O_3 particles in the CuNi(Al) coatings. The strengthening of CuNi(Al) cannot be explained by the formation of CuNi-Al_2O_3 composite coatings. Despite this, Al_2O_3 particles in the electrodeposition solution are responsible for the improved strength. Other strengthening mechanisms were investigated for a better understanding.

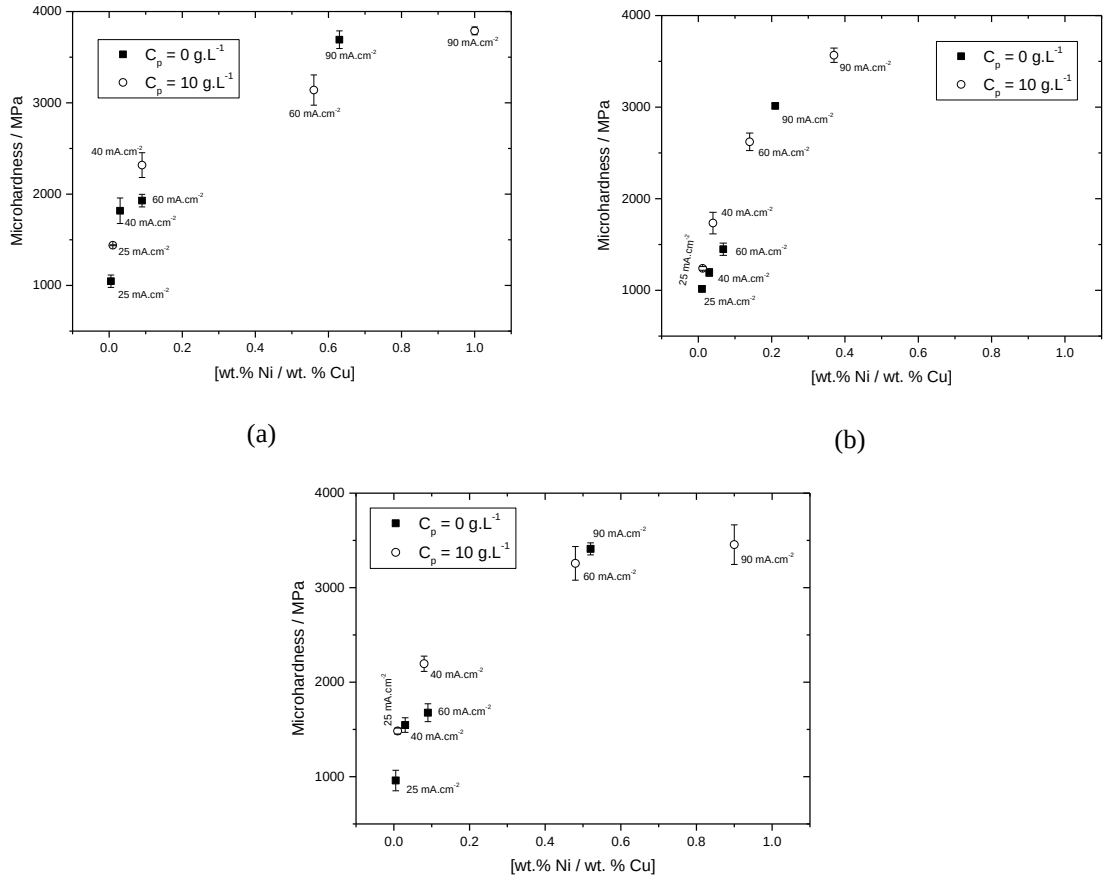

Figure 2. Microhardness as a function of i_g and Ni/Cu mass ratio of CuNi(w) and CuNi(Al) coatings: (a) near the top, (b) center, and (c) near the bottom edge.

Figure 3 condenses all values of microhardness. The dashed line in this figure corresponds to an ideal theoretical microhardness (MH_{CuNi}) of a CuNi alloy calculated as a linear superposition of individual unalloyed Cu and Ni microhardness (MH_{Cu} and MH_{Ni}), weighted by the mass fraction of the elements in the alloy (wt.% Cu and wt. % Ni) calculated by Eq. (1):

$$MH_{CuNi} = \frac{wt.\%\ Cu}{100} xMH_{Cu} + \frac{wt.\%\ Ni}{100} xMH_{Ni} \quad (1)$$

MH_{CuNi} corresponds to a simple ideal additive rule for a binary CuNi alloy. The results in Figure 3 are helpful to confirm the mechanism of hardening. As the values of MH for unalloyed Cu and Ni depend on many factors, these were taken from the standards for calibration and checking of microhardness testers´ performance of NIST ("NIST - Vickers Microhardness of Copper," n.d.; Vickers Microhardness of Nickel," n.d.) and are indicated in Figure 3. Note that Ni is considerably harder than Cu.

Figure 3 identifies three regions. The first one is at low i_g, where the coatings are richer in Cu. Here, experimental microhardness values tend to that for unalloyed Cu value (1226 MPa) and are close to MH_{CuNi}. The second one is above ca. 0.1 and up to 0.6 Ni/Cu ratio, with a positive deviation of experimental values compared to theoretical MH_{CuNi}. This deviation indicates solid-solution strengthening ("Foundry - Lexicon," n.d.). In this region, CuNi(Al) obtained at i_g of 40 and 60 $mA.cm^{-2}$ exhibited the highest microhardness and Ni/Cu mass ratio values than CuNi(w) at these same i_g. The third region corresponds to i_g 90 $mA.cm^{-2}$ for CuNi(Al) at the edges. These were the richest in Ni coatings, and experimental microhardness is very similar to the theoretical additive one. The significant content of the harder Ni metal determines microhardness behavior. Properties of the CuNi metal matrix can be tuned by a combination of i_g and Al_2O_3 particles in the electrodeposition solution, even with these not occluding in the matrix.

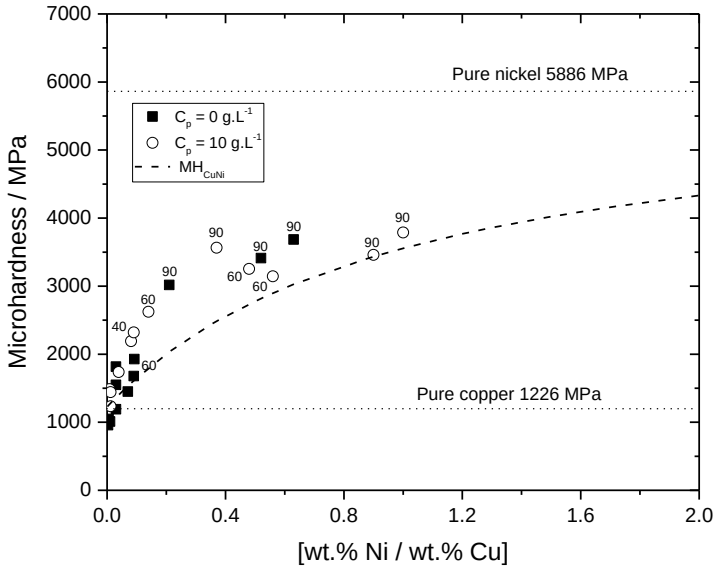

Figure 3. Compiled experimental values of microhardness of Figure 2 against Ni/Cu mass ratio. 90, 60 and 40 refer to i_g. Dashed line: theoretical additive microhardness according to Eq. (1). Values of unalloyed Cu and Ni are placed as references.

3.2 XRD analysis

XRD patterns of coatings obtained for distinct i_g and C_p are shown in Figure 4. CuNi forms a solid solution in the whole range of compositions with an fcc structure (ASM International and Handbook Committee, 2016), and the XRD patterns are very similar and typical for CuNi solid solution with fcc structure. The crystal plane (111) peak is the most intense. As expected from the EDS analysis, peaks related to Al_2O_3 are absent in the case of CuNi(Al). Peak positions depend on the composition of CuNi coatings, that is, of the Ni/Cu ratio. As the Ni atom is smaller than Cu, as the coating enriches in Ni, 2θ values of the peaks move toward larger values according to Bragg´s law. Analysis of XRD patterns in terms of compositional variation can give additional information about the reasons for strengthened CuNi(Al) coatings.

As a binary alloy that forms a solid solution in the whole range of compositions, compositional variation of CuNi with the XRD data can be explored in terms of Vegard´s law for random solid solutions (Ford et al., 2011; Lambregts and Frank, 2004; Zhao, 2007). According to the empirical Vegard´s law, the lattice parameter of a binary alloy, in this case, CuNi, is a weighted compositional average of those of pure metals:

$$a_{CuNi} = (1 - x_{Ni})a_{Cu} + x_{Ni}a_{Ni} \quad (2)$$

where a_{CuNi} is the lattice constant of CuNi solid solution, a_{Cu}, and a_{Ni} are the lattice constants of pure Cu (3.6148 Å) and pure Ni (3.5239 Å) (Cullity, 1978; Ford et al., 2011), respectively, and x_{Ni} and x_{Cu} the molar fraction of the elements in

the coatings taken from EDS data. Lattice constant (a_{CuNi}) can also be calculated independently from XRD patterns using the relation for *fcc* structures:

$$a_{hkl} = d_{hkl}\sqrt{h^2 + k^2 + l^2} \tag{3}$$

d_{hkl} is the interplanar spacing and, *h*, *k*, *l* are the Miller indexes (Cullity, 1978). The two calculated lattice constants can be plotted, and if Vegard´s law is followed, a very near 1:1 relation must be obtained. This was initially made by considering only the (111) crystal plane peak, resulting in a large dispersion of the points. The dispersion was due to considering only one peak from the XRD patterns. For a more accurate determination of a_{CuNi} from XRD patterns, it is recommended that several diffraction peaks must be considered, and not only one, especially for high diffraction angles where better accuracy is obtained. This determination is accomplished by the Nelson-Riley function (f_{NR}), which relates the calculated a_{CuNi} with an expected precision (Ford et al., 2011; Ghosh et al., 2000):

$$\frac{\Delta a}{a_{hkl}} = k\left(\frac{\cos\theta_{hkl}^2}{\sin\theta_{hkl}} + \frac{\cos\theta_{hkl}^2}{\theta_{hkl}}\right) = f_{NR} \tag{4}$$

a_{hkl} from Eq. (3) is obtained for each diffraction peak, and f_{NR} is calculated. A plot of a_{hkl} *vs.* f_{NR} should be a straight line, and the intercept at $f_{NR} = 0$ will furnish the corrected lattice constants ($a_{CuNi,NR}$) since $\Delta a/a$ goes to zero. Four peaks were taken related to crystal planes (111), (200), (220), and (311) for each i_g and C_p in the XRD patterns. Figure 5 shows an example of Nelson-Riley function plot.

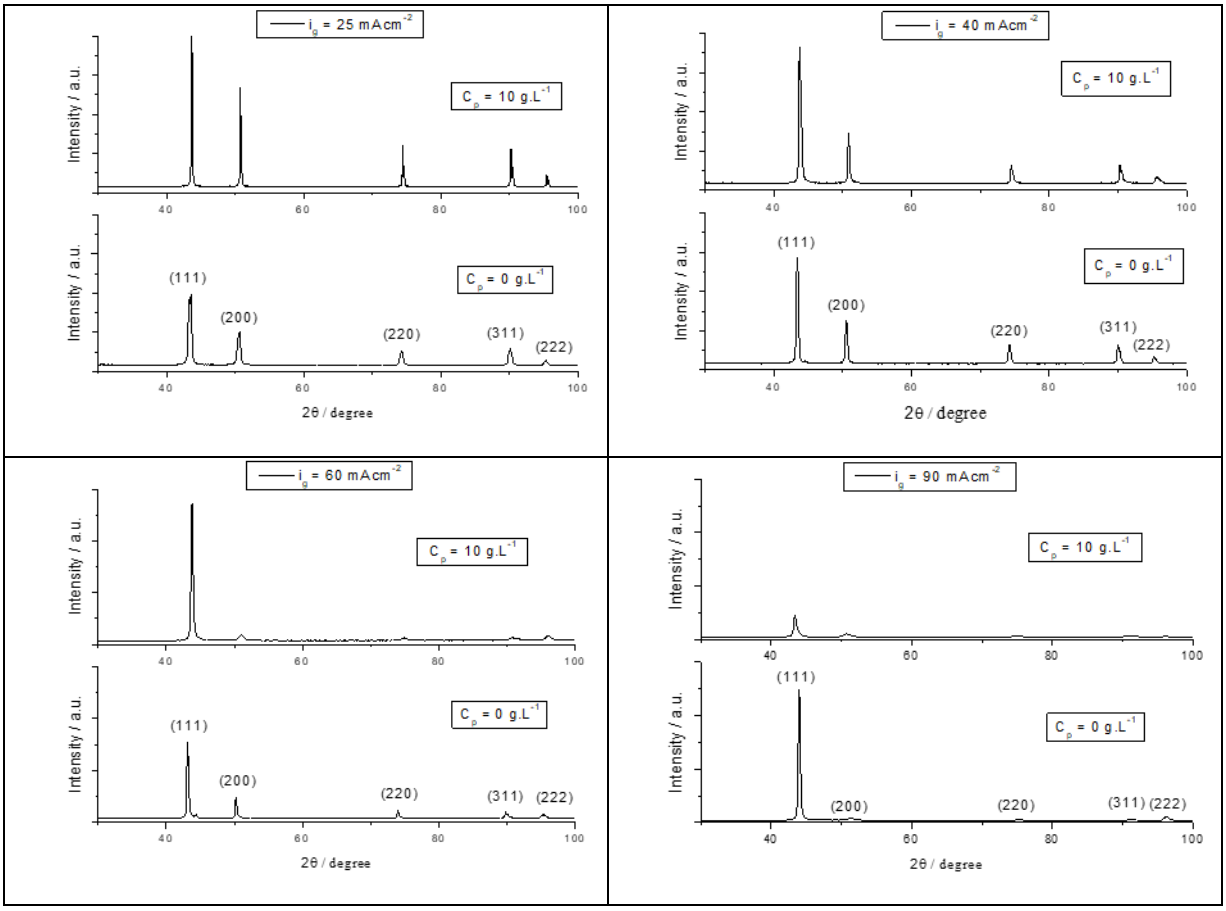

Figure 4: XRD patterns for CuNi(Al) and CuNi(w) coatings obtained at distinct i_g indicated.

The corrected $a_{CuNi,NR}$ for each CuNi coating and current density was plotted against $a_{CuNi,EDS}$ (from Eq. (2)) in Figure 6. The values are close to Vegard´s law reference line up to CuNi(w) at i_g 60 mA.cm^{-2}. However, there is a negative deviation from this law for CuNi(Al) at 60 and 90 mA.cm^{-2} and for CuNi(w) at 90 mA.cm^{-2}. Reasons for deviations from Vegard´s law are out of the scope of this work. The results in Figure 6 are, however, in agreement with the fact that Ni is smaller than Cu and that coatings CuNi(Al) for i_g 60 and 90 mA.cm^{-2} and CuNi(w) for 90 mA.cm^{-2} exhibit higher Ni/Cu mass ratios and microhardness as shown in Figures 2 and 3.

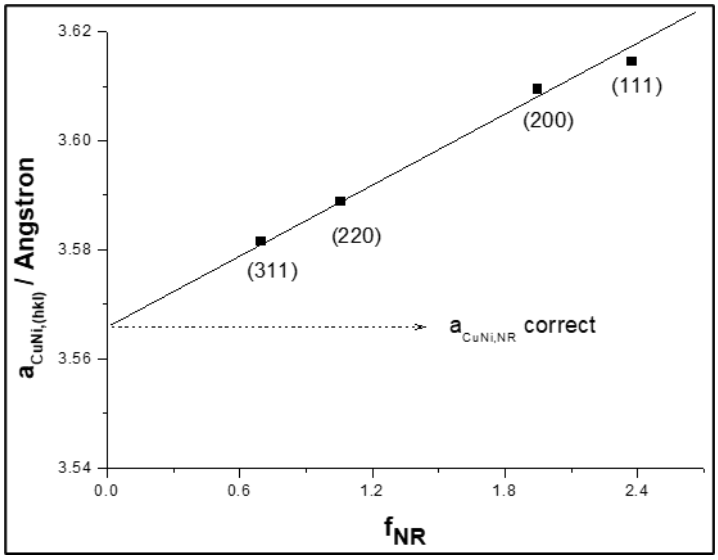

Figure 5: A Nelson-Riley plot for a CuNi(Al) coating at i_g of 90 mA.cm^{-2}. Miller indexes of the planes for each point are indicated.

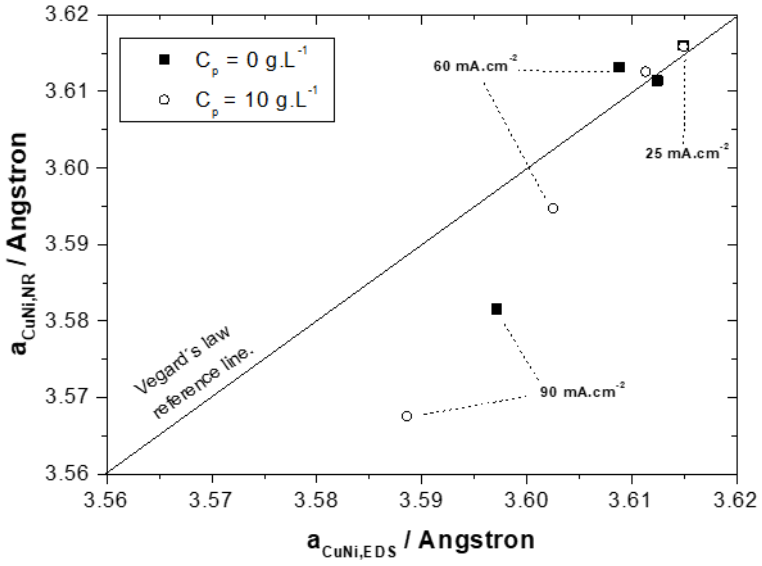

Figure 6: Plot of corrected $a_{CuNi,NR}$ from Nelson-Riley against $a_{CuNi,EDS}$.

In Figure 7, the corrected lattice parameters of CuNi taken from XRD patterns ($a_{CuNi,NR}$) are plotted against i_g for CuNi(w) and CuNi(Al). The trend of decreasing $a_{CuNi,NR}$ of this with i_g for all conditions is clearly seen, as expected. As i_g increases, higher negative overpotentials are attained during electrodeposition, favoring Ni^{2+} reduction. For i_g 25 and 40 mA.cm^{-2} no differences are seen between CuNi(w) and CuNi(Al). However, for 60 and 90 mA.cm^{-2}, smaller values of $a_{CuNi,NR}$ for CuNi(Al) are seen compared to CuNi(w), which is a more unambiguous indication of the enrichment in Ni in the coatings at high i_g when Al_2O_3 particles are in the electrodeposition solution, which, in conjunction with solid-solution hardening and highest harder Ni content at 90 mA.cm^{-2} explains the highest microhardness of the CuNi(Al) coatings, corroborating the analysis made in Figure 3.

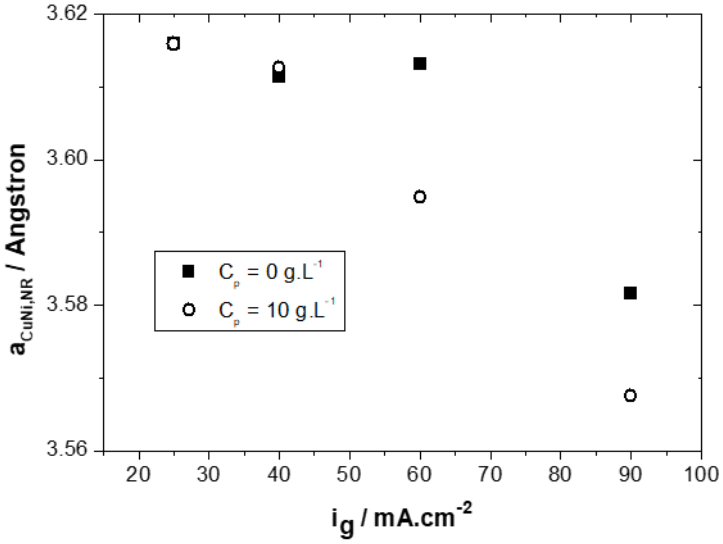

Figure 7: Plot of corrected $a_{CuNi,NR}$ *vs.* i_g for CuNi(w) and CuNi(Al).

4. CONCLUSIONS

Copper-nickel coatings obtained by electrodeposition from Al_2O_3 particles containing citrate-ammonia solutions pH 9.2 exhibited improved mechanical strength than those obtained at the same conditions without Al_2O_3 in the electrodeposition solution. Improvement was observed at high i_g of 40, 60, and 90 mA.cm^{-2}. No occlusion of Al_2O_3 was observed.

The mechanism of strengthening was investigated using XRD and EDS, and the characteristics of complete miscibility of CuNi. When Al_2O_3 particles are in the electrodeposition solution, there is a significant increase in Ni content. Solid-solution strengthening and the harder Ni content in CuNi(Al) matrix explain the results.

Micrometric particles of Al_2O_3, when in the electrodeposition solution of CuNi can tune the mechanical properties of these coatings by changing CuNi composition.

5. ACKNOWLEDGEMENTS

The authors thank CNPq (Conselho Nacional de Pesquisa e Desenvolvimento) for the financial support.

6. REFERENCES

About nickel | Nickel Institute [WWW Document], n.d. URL https://nickelinstitute.org/en/about-nickel-and-its-applications/ (accessed 5.19.22).

Alizadeh, M., Safaei, H., 2018. Characterization of Ni-Cu matrix, Al2O3 reinforced nano-composite coatings prepared by electrodeposition. Applied Surface Science 456, 195–203. https://doi.org/10.1016/j.apsusc.2018.06.095

ASM International, Handbook Committee, 2016. ASM Handbook. Volume 3.

Bigos, A., Wolowicz, M., Janusz-Skuza, M., Starowicz, Z., Szczerba, M.J., Bogucki, R., Beltowska-Lehman, E., 2021. Citrate-based baths for electrodeposition of nanocrystalline nickel coatings with enhanced hardness. Journal of Alloys and Compounds 850, 156857. https://doi.org/10.1016/j.jallcom.2020.156857

Callister, W.D., 2007. Materials science and engineering: an introduction, 7th ed. ed. John Wiley & Sons, New York.

Chassaing, E., Quang, K.V., Wiart, R., 1987. Mechanism of copper-nickel alloy electrodeposition. J Appl Electrochem 17, 1267–1280. https://doi.org/10.1007/BF01023611

Cullity, B.D., 1978. Elements of x-ray diffraction, 2d ed. ed, Addison-Wesley series in metallurgy and materials. Addison-Wesley Pub. Co, Reading, Mass.

Fawzy, M.H., Ashour, M.M., Abd El-Halim, A.E.-H.M., 1996. Effect of Some Operating Variables on the Characteristics of Electrodeposited Cu-Ni Alloys with and without α-Al2O3 and TiO2 Inert Particles. J. Chem. Technol. Biotechnol. 66, 121–130. https://doi.org/10.1002/(SICI)1097-4660(199606)66:2<121::AID-JCTB475>3.0.CO;2-A

Ford, M., Nill, M., Bryant, A., 2011. [PDF] Lab 03: Precision X-Ray Diffractometry - Free Download PDF [WWW Document]. URL https://silo.tips/download/lab-03-precision-x-ray-diffractometry (accessed 6.16.22).

Foundry - Lexicon [WWW Document], n.d. URL https://www.giessereilexikon.com/en/foundry-lexicon/Encyclopedia/show/strengthening-mechanisms-4698/?cHash=a1de8b3f251a87d649ec6d341ee39d8d,

https://www.giessereilexikon.com/en/foundry-lexicon/Encyclopedia/show/strengthening-mechanisms-4698/ (accessed 5.19.22).
Foyet, A., Hauser, A., Schäfer, W., 2007. Double template electrochemical deposition and characterization of NiCo and NiCu alloys nanoparticles and nanofilms. J Solid State Electrochem 12, 47–55. https://doi.org/10.1007/s10008-007-0332-2
Friend, W.Z., 1980. Corrosion of nickel and nickel-base alloys, The Corrosion monograph series. Wiley, New York.
Ghosh, S.K., Grover, A.K., Dey, G.K., Totlani, M.K., 2000. Nanocrystalline Ni–Cu alloy plating by pulse electrolysis. Surface and Coatings Technology 126, 48–63. https://doi.org/10.1016/S0257-8972(00)00520-X
Hovestad, A., Janssen, L.J.J., 2005. Electroplating of Metal Matrix Composites by Codeposition of Suspended Particles, in: Conway, B.E., Vayenas, C.G., White, R.E., Gamboa-Adelco, M.E. (Eds.), Modern Aspects of Electrochemistry, Modern Aspects of Electrochemistry. Springer-Verlag, New York, pp. 475–532. https://doi.org/10.1007/0-387-25838-8_6
Kear, G., Barker, B.D., Stokes, K., Walsh, F.C., 2004. Electrochemical Corrosion Behaviour of 90–10 Cu–Ni Alloy in Chloride-Based Electrolytes. Journal of Applied Electrochemistry 34, 659–669. https://doi.org/10.1023/B:JACH.0000031164.32520.58
Lambregts, M.J., Frank, S., 2004. Application of Vegard's law to mixed cation sodalites: a simple method for determining the stoichiometry. Talanta 62, 627–630. https://doi.org/10.1016/j.talanta.2003.09.007
Lozano-Morales, A., Podlaha, E.J., 2008. Electrodeposition of NiCu-matrix nanocomposites using a rotating cylinder Hull cell. J Appl Electrochem 38, 1707–1714. https://doi.org/10.1007/s10800-008-9620-5
Monel | alloy | Britannica [WWW Document], 2007. URL https://www.britannica.com/technology/Monel (accessed 5.19.22).
NIST - SRM Order Request System SRM 1894a - Vickers Microhardness of Copper [WWW Document], n.d. URL https://www-s.nist.gov/srmors/view_detail.cfm?srm=1894A (accessed 7.20.22).
NIST - SRM Order Request System SRM 1896b - Vickers Microhardness of Nickel [WWW Document], n.d. URL https://www-s.nist.gov/srmors/view_detail.cfm?srm=1896B (accessed 7.20.22).
Panda, A., Podlaha, E.J., 2003. Nanoparticles to Improve Mass Transport Inside Deep Recesses. Electrochem. Solid-State Lett. 6, C149. https://doi.org/10.1149/1.1614452
Tseluikin, V.N., 2016. On the Structure and Properties of Composite Electrochemical Coatings. A Review. Prot Met Phys Chem Surf 52, 254–266. https://doi.org/10.1134/S2070205116010251
Zhao, J.-C. (Ed.), 2007. Methods for phase diagram determination. Elsevier, Amsterdam ; New York.

7. RESPONSIBILITY NOTICE

The authors are the only ones responsible for the printed material included in this paper.